

Rotationally Symmetrical Spoof-Plasmon Antenna for Polarization-Independent Radiation Enhancement

Xin Zheng,^{1,2} Jingjing Zhang,^{1,2,*} Yu Luo^{1,2},^{3,4} Zhengxing Wang,^{1,2} Yi Ren^{1,2} and Tie Jun Cui^{1,2}

¹*Institute of Electromagnetic Space, Southeast University, Nanjing 210096, China*

²*State Key Laboratory of Millimeter Waves, Southeast University, Nanjing 210096, China*

³*School of Electrical and Electronic Engineering, Nanyang Technological University, Nanyang Avenue 639798, Singapore*

⁴*UMI 3288 CINTRA, CNRS/NTU/THALES, Nanyang Technological University, 50 Nanyang Drive, Singapore 637553, Singapore*

(Received 2 May 2022; revised 16 September 2022; accepted 3 October 2022; published 7 November 2022)

Plasmon antennas allow subwavelength confinement and enhancement of electromagnetic fields at the “hotspot” where the radiation efficiency of emitters can be substantially enhanced. Such enhancement, however, is often polarization dependent. Consequently, the radiation behaviors (e.g., radiation pattern and polarization states) of the emitter placed at the hotspot are also modified significantly. Enhancing the radiation efficiency without altering the original radiation pattern and polarization state of the emitter is highly desired for many sought-after applications involving chiral emitters but remains a challenging task, especially at low frequencies. To this end, spoof-plasmon antennas with fourfold and sixfold rotational symmetries are designed and realized experimentally. These plasmon antennas support polarization-independent localized plasmon resonances, which can significantly enhance the local density of photonic states at the structural center without changing the polarization state of the emitter. As a typical example, the structure with sixfold rotational symmetry is coupled with a half-wave dipole antenna. The measurement results show that the far-field radiation pattern of the dipole antenna is maintained with the radiation efficiency enhanced by more than 2 orders of magnitude, irrespective of the dipole orientation.

DOI: 10.1103/PhysRevApplied.18.054018

I. INTRODUCTION

The ability to tailor the spontaneous emission of quantum emitters is of paramount importance for nanophotonic research, attracting intense attention from both scientists and engineers over the past few decades [1,2]. Suggested by Purcell, the spontaneous emission rate is proportional to the local density of states (LDOS), both of which can be precisely engineered by changing the environment of the quantum emitter. Plasmon antennas [3] supporting localized-surface-plasmon (LSP) resonances offer a possible route towards this goal. Typical examples include dimer structures, wedges and grooves, chains of nanoparticles, and plasmon clusters [4–12]. These structures can concentrate light energy at the deep subwavelength scale, generating a “hotspot” where the local electromagnetic field, and hence, the LDOS, is enhanced by orders of magnitude. In this way, the radiation efficiency of emitters located at the hotspots can be substantially enhanced, through the coupling of the emitters with plasmon antennas [13–15]. This remarkable feature is of fundamental

interest for a wide range of applications, including surface-enhanced Raman spectroscopy [16], photovoltaics [17], nonlinear processes [18], and surface-enhanced fluorescence [19].

Although the plasmon-enhanced emission is widely studied at optical frequencies, its low-frequency counterpart is rarely explored. In 2004, Pendry *et al.* showed that patterned metal surfaces with periodic corrugations supported surface electromagnetic modes in microwave and terahertz spectra, with dispersion akin to that of surface-plasmon polaritons at optical frequencies [20]. This concept, later named as spoof plasmonics, offers a powerful platform to transfer useful applications of optical plasmons to low frequencies [21–41]. In addition, the spoof-plasmon concept can be applied on closed surfaces to mimic LSP resonances [21–27], which, through proper engineering, give rise to giant enhancement of the local electric fields [28–30], holding promise for sensing applications at low frequencies [31–33]. When applied to radiation enhancement [34–38], however, these structures show some distinct drawbacks. First, excitation of the spoof LSP modes in these structures is generally restricted to a specific polarized incidence. Take the spiral dimer [29] and the bowtie

*zhangjingjing@seu.edu.cn

structure [39,40] as examples, only the incident electric field oriented along the long axis of the structure can be enhanced. When coupled with circularly polarized emitters, these structures change the polarization state of the source antenna, while enhancing the radiation efficiency, converting the emitted circular polarization into the linear one. Second, even considering only coupling with linearly polarized dipole antennas, these structures may still significantly modify the original radiation pattern of the source antenna, since only the emission perpendicular to the structural axis is allowed. On the other hand, many wireless communication scenarios (e.g., satellite communications) require circular polarization from chiral emitters. Other applications, such as radar and radio-frequency identification, require radiation enhancements without changing the radiation pattern of the emitter. In other words, the polarization-dependent radiation feature is the bottleneck problem that prevents spoof LSP enhancements from these applications.

To tackle this challenge, we consider spoof-plasmon antennas with fourfold and sixfold rotational symmetries. We demonstrate experimentally that our proposed spoof-plasmon antennas can achieve giant field enhancements for unpolarized light, regardless of the excitation direction. Our measurements show that a half-wave dipole antenna coupled with the proposed spoof-plasmon structures can radiate at a frequency much lower than the fundamental resonance frequency of the dipole. The corresponding radiation enhancements for C_4 - and C_6 -symmetric structures reach 30 and 200, respectively, while the far-field radiation pattern of the dipole is maintained, irrespective of its relative orientation with respect to the spoof-plasmon structure. The cross-resonant optical antenna with C_4 symmetry is theoretically demonstrated to be a good

candidate able to convert radiation from an emitter of any polarization state into correspondingly polarized propagating fields [41]. However, the direct experimental realization of emission enhancements from such an antenna has never been reported, to the best of our knowledge. Our study gives concrete proof that spoof-plasmon structures with higher-fold ($n \geq 4$) rotational symmetries provide a possible route to polarization-independent radiation management, and our design scheme can be easily extended to other geometries at any frequency range. The designed spoof-plasmon antennas are not restricted to enhance the radiation of the dipole antenna, but can work with, in principle, a general class of more complicated antennas for various applications.

II. RESULTS AND DISCUSSION

Figure 1 gives the schematic of the proposed structures, which are composed of four or six spoof-plasmon waveguides arranged in a rotationally symmetric manner. Each waveguide consists of a corrugated metal (copper) strip and an equilateral triangle taper. The metal has a thickness of 0.035 mm, and the rest of the geometrical parameters marked in Fig. 1 are set as $L = 50$ mm, $W = 15$ mm, $w_2 = 6.76$ mm, $h = 1$ mm, $w_3 = 7.16$ mm, $\beta = 3^\circ$, and $R_{i+1}/R_i = k^{0.5}$, with $i = 1, 2, 3, \dots, 10$, $R_1 = 12.99$ mm, and $k = 0.85$. The depth of the corrugations affects the resonance frequency. The electric field density at the center is detected by a probe, which is used as a measurable index. These geometric parameters are obtained by the global optimization with the objective to achieve better field-localization performance. The design of a cross-shaped spoof-plasmon antenna (or spoof-plasmon tetramer structure) is inspired by the principle that any arbitrary

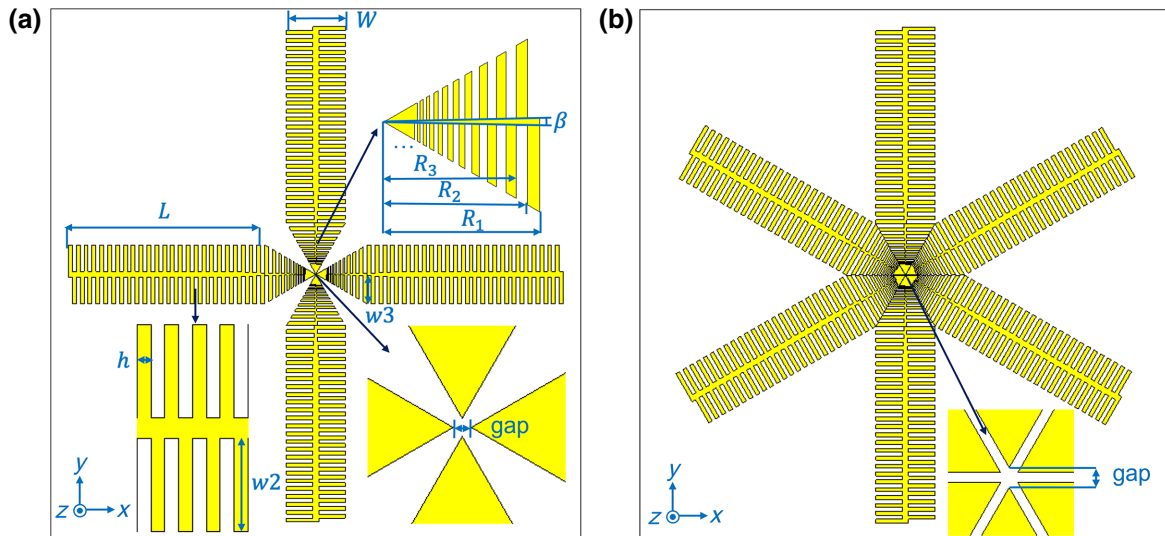


FIG. 1. Simulated model of the designed spoof-plasmon structure with (a) fourfold and (b) sixfold mirror symmetry. Sample consists of copper structures on top of a dielectric layer made of Rogers 5880, the thicknesses of which are 0.035 and 0.508 mm, respectively.

polarization state carried by a transverse propagating electromagnetic wave in the horizontal plane of the structure can be decomposed into mutually orthogonal components. The superposition of resonant modes excited by the two orthogonal components of the electromagnetic fields leads to further enhancements of local electric fields at the common feed gap, while the relative phase between the field components remains unchanged [41]. The sixfold symmetric structure (or spoof-plasmon hexamer structure) in Fig. 1(b) is designed for the purpose of adding more resonant components. In the hexamer case, the adjacent equilateral triangle tips form a narrow slit of 0.05 mm,

and in both tetramer and hexamer cases, the gap size (as denoted in Fig. 1) between the facing taper tips is set as 0.1 mm.

In the numerical simulations performed using the commercial software CST Studio Suite, Rogers 5880 with a thickness of 0.508 mm is chosen as the substrate. We first use linearly polarized plane waves propagating parallel to the substrate, the electric field density of which is set as 1 V/m, to excite the resonances on the spoof-plasmon antennas, where the incident polarization is given in the insets of Figs. 2(a) and 2(c). The field enhancements at the structural center versus the frequency under

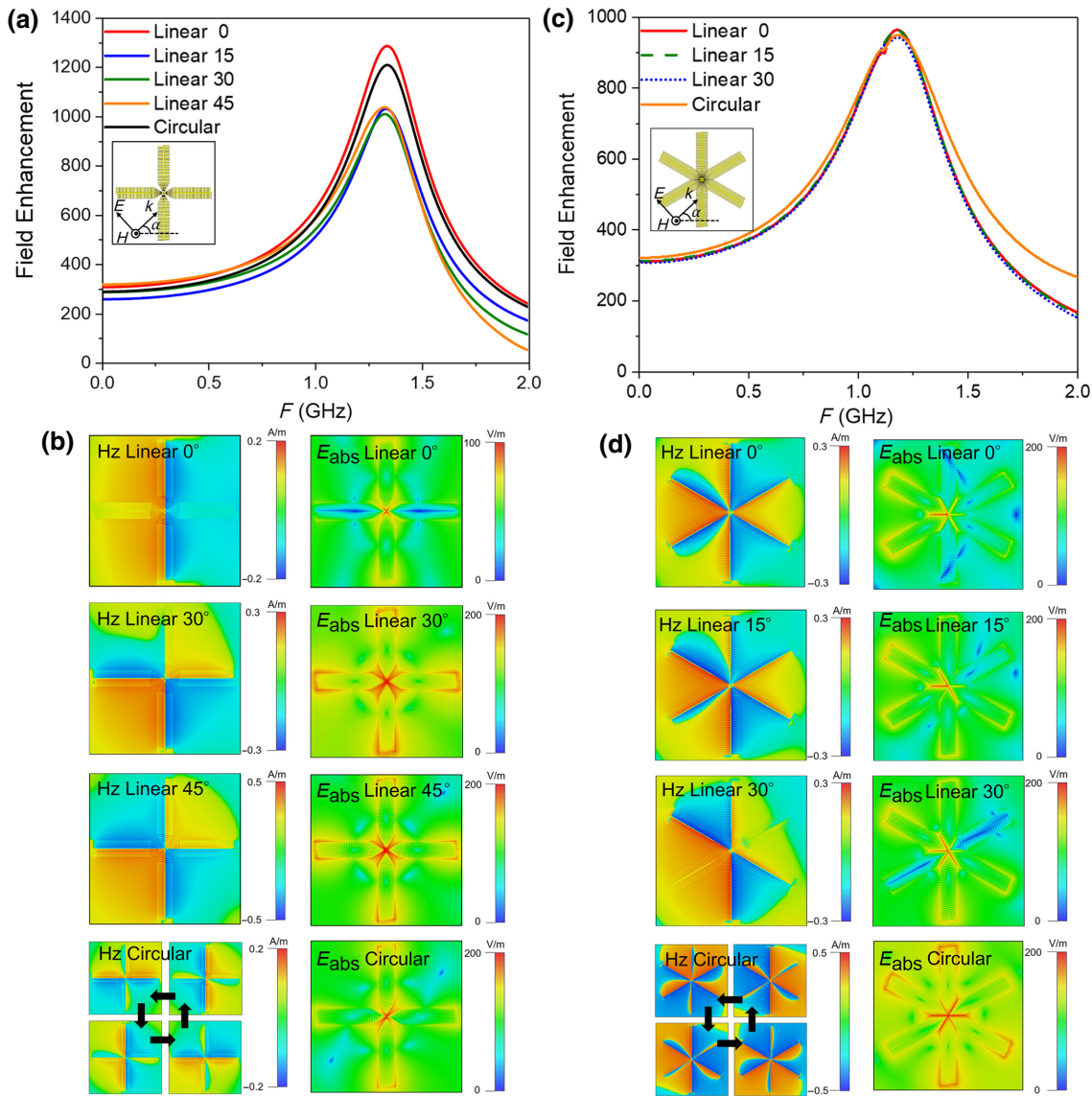


FIG. 2. (a) Electric field enhancement at the center of the spoof-plasmon tetramer structure under excitation of linearly polarized waves from different angles and circularly polarized wave perpendicularly incident on the structure. (c) Electric field enhancement at the center of the spoof-plasmon antenna with sixfold symmetry under excitation of linearly polarized waves from different angles and circularly polarized wave perpendicularly incident on the structure. (b),(d) z component of magnetic field and corresponding absolute value of electric field intensity in the plane $z = -0.2365$ mm. Those panels under excitation of the circular polarization wave are taken at every quarter of a period.

different excitation angles, α (i.e., the angle between the illumination direction and the horizontal arm), are simulated and compared. Owing to the C_4 symmetry of the geometry, we consider only the excitation angle, α , varying from 0° to 45° . As shown in Fig. 2(a), a peak of the local field enhancement occurs at 1.33 GHz, corresponding to the dipolar resonance of the spoof-plasmon antenna. The corresponding resonance-mode profiles under different illumination angles are plotted in Fig. 2(b). The distribution of the z component of the magnetic field, displayed in the left column of Fig. 2(b), shows that, when $\alpha = 0^\circ$, only the dipolar resonance along the vertical direction can be excited, similar to the case of a dimer structure [29]. The absolute value of the electric field plotted in the right column of Fig. 2(b) indicates that a hotspot is generated at the center of the structure, where the field is strongly localized and enhanced. As the incident direction is tilted to 30° and 45° , the dipolar resonances along both the horizontal and vertical directions are excited, giving rise to a quadrupolelike mode, the excitation of which is insensitive to the angle α . To further illustrate the polarization-independent responses, we consider a left-handed circularly polarized wave incident perpendicularly upon the structure and plot the snapshots of hertz (Hz) in one oscillation period. The dynamic response shows that the field patterns rotate in the counterclockwise direction with circular dichroism similar to that of the incident wave. Such a near-field distribution is a typical characteristic of the circular dipole resonance and an enormous field enhancement of up to 1286 is obtained at the structural center. By comparing the results shown in Fig. 2(a), we note small variations of the maximum field enhancement at the hotspot under different incident polarizations, ranging from 1008 to 1286. For the spoof-plasmon hexamer structure, as shown in Fig. 2(c), a peak of the local field enhancement occurs at 1.17 GHz, corresponding to the quadrupolelike resonance of the spoof-plasmon antenna. The corresponding resonance-mode profiles under different illuminations angles are plotted in Fig. 2(d). The distribution of the z component of the magnetic field, displayed in the left column of Fig. 2(d), shows that, for 30° incidence, only the dipolar resonance along the axis of the other four waveguides can be excited, similar to the case of a tetramer structure. As the incident angle is tilted to 0° and 15° , the dipolar resonances along the axes of all waveguides are excited, the excitation of which is insensitive to the angle. Similar to the results for C_4 symmetry, a hotspot can be observed at the center of the structure, according to the right column in Fig. 2(d).

Both spoof-plasmon structures proposed above can increase the LDOS, giving rise to significant radiation enhancement of emitters presented at the feed gap. According to the theory of reciprocity, the polarization-independent responses make the proposed structures capable of enhancing the emission rate of the

antenna, while preserving its far-field radiation pattern and polarization state. To verify this feature, we experimentally investigate the radiation of a half-wave dipole antenna (DA) located at the gap of the structures. The geometrical parameters of the fabricated samples are the same as those in the simulations, except that the gap size between the triangular tips is changed to 1.4 mm. The material of the dielectric layer is changed to Rogers 4003C for its higher hardness, and the thickness of the substrate is set as 0.508 mm. An emitter (half-wave dipole) with a length of 60 mm and width of 0.4 mm is placed at the center of the structure (see the insets of Fig. 3) and connected with the coaxial cable.

Emitters with different orientations ($\alpha = 35^\circ$, 40° , and 45°) are coupled with the spoof-plasmon antenna, and the corresponding emission rate enhancements and far-field radiation patterns are investigated. To highlight the advantages of the proposed structures, the spoof-plasmon DS is introduced as a reference for comparison. The first column of Fig. 3 plots S11 parameters for the dipolar antenna with (red and blue lines) and without (orange and green lines) the dimer structure. Through coupling with the spoof-plasmon structure, the dimer structure shows a dip in its S11 spectrum at around 1.1 GHz, far below the fundamental resonance frequency of a bare dipolar antenna. However, the polarization-dependent resonance nature makes the depth of the S11 dip change with α . In sharp contrast, the spoof-plasmon TS displayed in the second column of Fig. 3 shows an S11 dip at around 1.08 GHz, the strength of which is insensitive to the dipole orientation. The polarization-independent emission property of the spoof-plasmon tetramer structure is further illustrated in the right column of Fig. 3, where we simulate and compare the spectra of the total radiation enhancement (i.e., the efficiency of the dipolar antenna in the presence of the spoof-plasmon structures normalized by that of a bare emitter) for the two spoof-plasmon structures under different dipole orientations. At $\alpha = 35^\circ$, the tetramer structure can enhance the radiation efficiency of the dipole by a factor of around 30, which only slightly decreases to 20 when α increases to 45° . On the contrary, the radiation enhancement for the dimer structure decreases swiftly from 30 to less than 10 when α increases from 35° to 45° . See supplemental material [42] for more simulated results of other angles.

To demonstrate that the tetramer structure preserves the far-field radiation properties of the dipole emitter, we simulate three-dimensional (3D) radiation patterns [i.e., left panels of Figs. 4(a)–4(f)] and measure E [i.e., middle panels of Figs. 4(a)–4(f)] and H planes [i.e., right panels of Figs. 4(a)–4(f)] of radiation patterns for the two coupled systems studied in Fig. 3. Figures 4(a)–4(c) show that the radiation of the dipolar-antenna–dimer-structure coupled system is fixed at a direction perpendicular to the dimer axis, irrespective of the dipole orientation, i.e., the far-field pattern is barely changed, as the excitation angle, α , varies

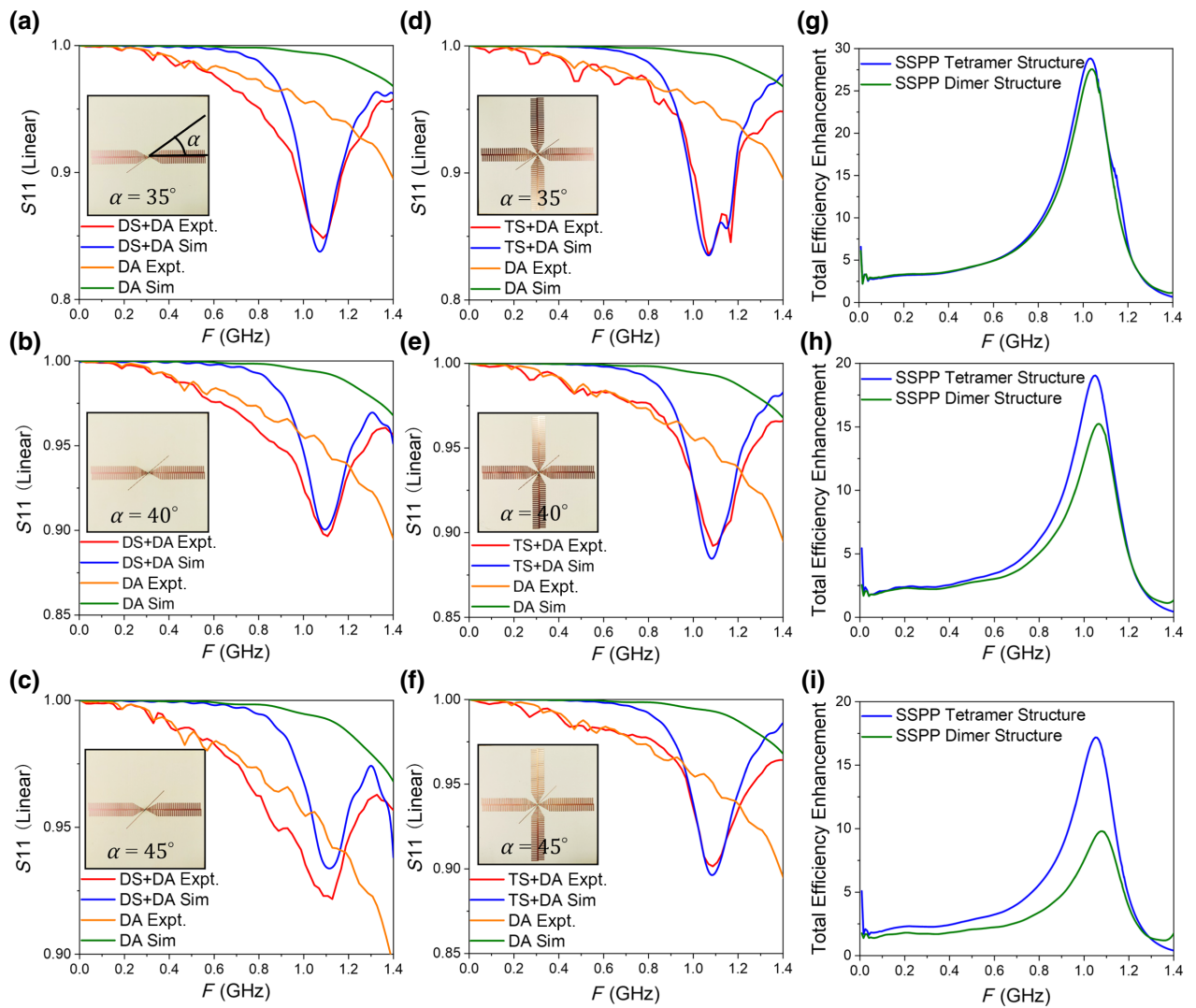


FIG. 3. (a)–(c) Simulated and measured S_{11} parameters of the bare half-wave DA and that coupled with the spoof-plasmon dimer structure (DS) under different excitation angles of $\alpha = 35^\circ$, 40° , and 45° , respectively, from top to bottom. (d)–(f) Simulated and measured S_{11} parameters of the bare DA and that coupled with the spoof-plasmon tetramer structure (TS) under different excitation angles of $\alpha = 35^\circ$, 40° , and 45° , respectively, from top to bottom. (g)–(i) Enhancement of total radiation efficiency versus frequency for the tetramer structure and dimer structure.

from 35° to 40° and 45° . In sharp contrast, Figs. 4(d)–4(f) show that, when the half-wave dipolar antenna is coupled with the tetramer structure, the far-field radiation pattern and the polarization state changes according to the dipole orientation, without being perturbed by the presence of the tetramer structure in the near field. We remark that the far-field radiation pattern is slightly different from that of an ideal dipolar antenna because the LDOS and radiation enhancements by the tetramer structure are not completely polarization independent, as evidenced in Fig. 2(a) and Figs. 3(g)–3(i).

To make the radiation-enhancement property more robust to the emitter orientation, we next couple the dipole emitter to the spoof-plasmon structure with sixfold

rotational symmetry. The schematic of the fabricated sample is given in Fig. 5(a) with the dipolar antenna orientated at $\alpha = 60^\circ$. The simulated (blue and green lines) and measured (red and orange lines) S_{11} spectra of the bare dipolar antenna and the coupled system is depicted in Fig. 5(b). We find that the coupling with the spoof LSP HS leads to even smaller reflection at the resonant frequency, as compared to the tetramer case. Although the field enhancement at the structural center of the hexamer is smaller than that of the tetramer structure, the two slits allow stronger coupling of the dipole to the spoof-plasmon antenna, leading to higher enhancement of the radiation efficiency. As shown in Fig. 5(c), an enhancement factor of almost 200 is obtained. Note that an extra dip, induced by the

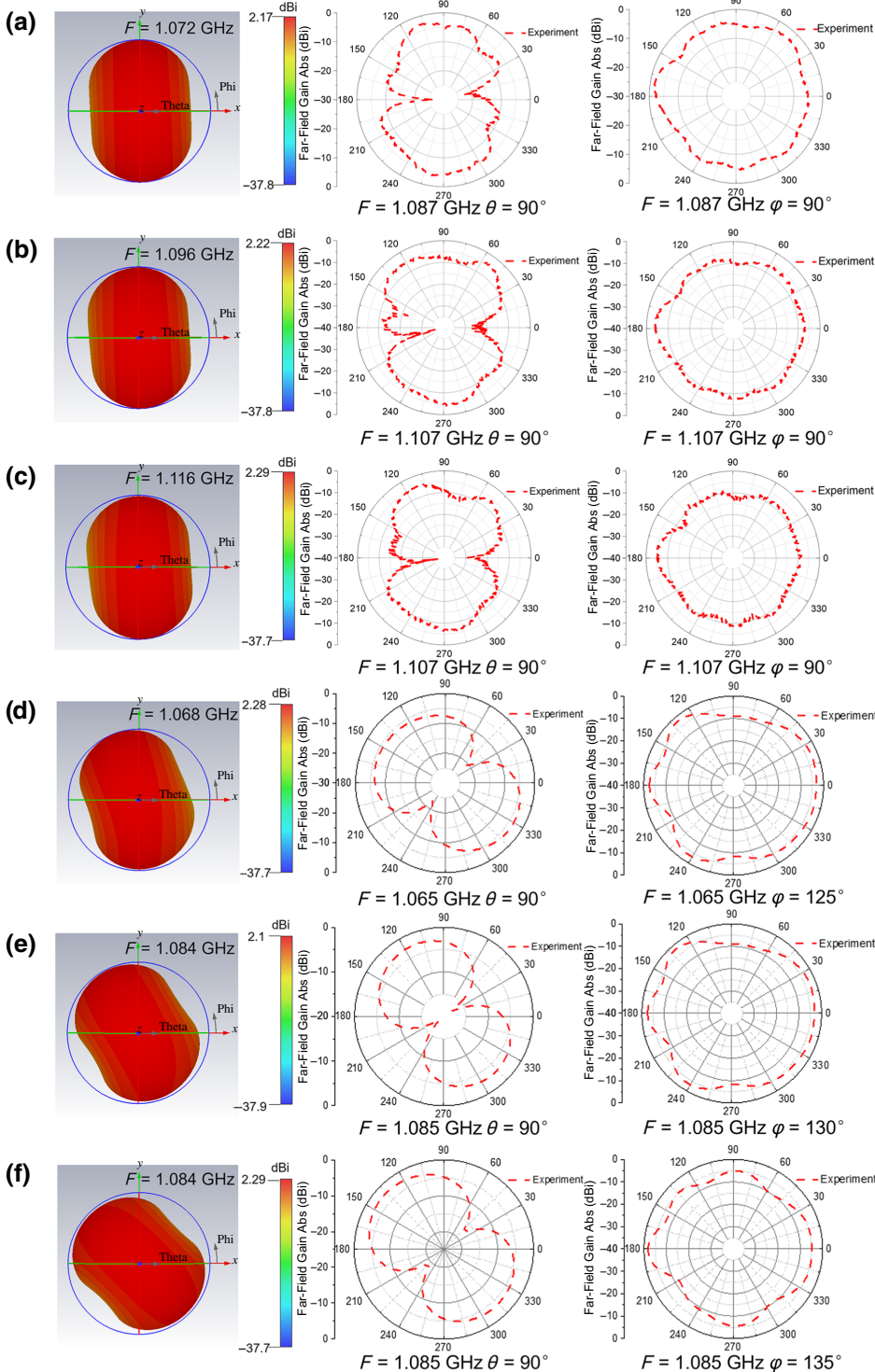


FIG. 4. (a)–(c) Simulated 3D radiation patterns (left column) and measured E planes (middle column) and H planes (right column) of radiation patterns when the half-wave dipolar antenna is coupled with the spoof-plasmon dimer structure. From top to bottom, the excitation angle, α , is set as 35° , 40° , and 45° , respectively. (d)–(f) Simulated 3D radiation patterns and measured E and H planes of radiation patterns when the half-wave dipolar antenna is coupled with the spoof-plasmon tetramer structure, where, from top to bottom, the excitation angle, α , is set as 35° , 40° , and 45° , respectively.

interference between the dipole antenna and the adjacent spoof-plasmon waveguides, appears on the S_{11} spectrum next to the main resonance dip. In fact, a similar phenomenon is also observed in Fig. 3(d), where an extra dip shows when the dipole antenna gets closer to the horizontal spoof-plasmon waveguide. The difference between the simulated and measured magnitude and frequency in

Fig. 5(b) results from extra loss in the experiment and the impedance mismatch between the fabricated sample and the feeding electronic circuit. The polarization-independent characteristic of this spoof-plasmon hexamer structure is also demonstrated by the simulated and measured far-field radiation patterns displayed in Figs. 5(d)–5(f).

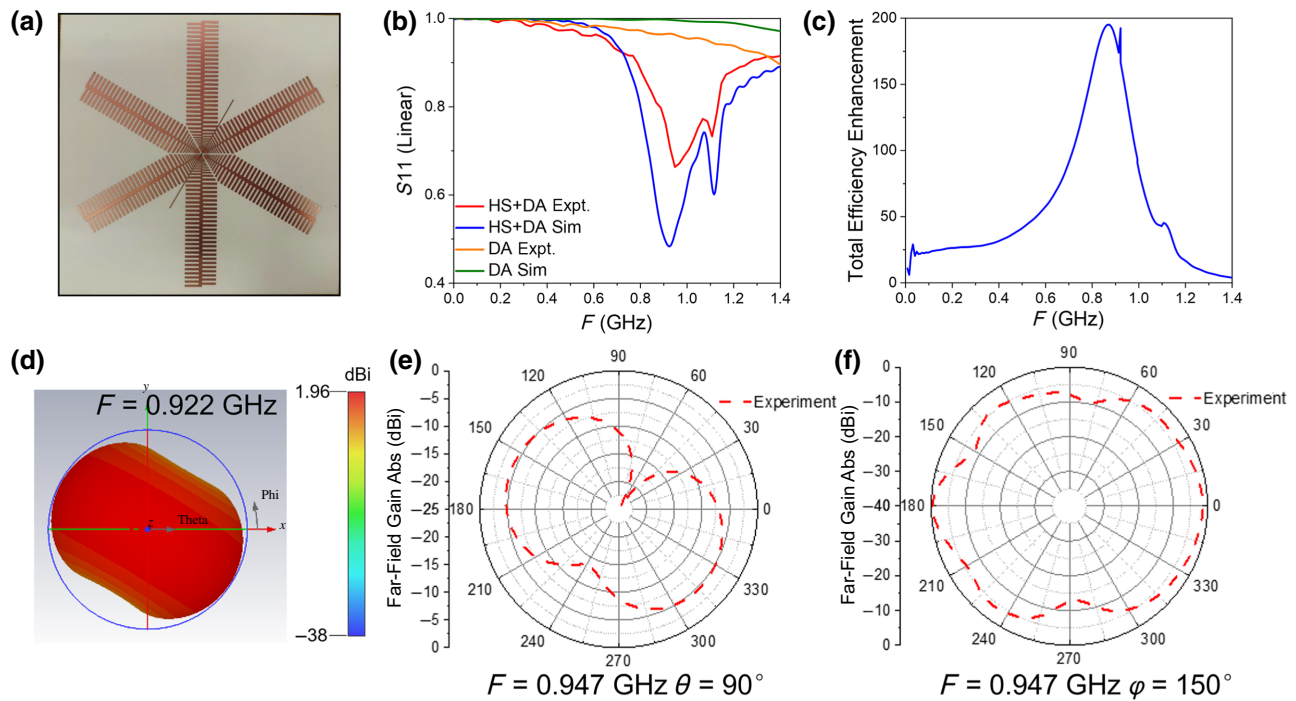


FIG. 5. (a) Fabricated sample of half-wave dipole coupled with a spoof-plasmon antenna with sixfold rotational symmetry. (b) Simulated and measured S₁₁ parameters of the bare half-wave dipolar antenna and that coupled with the spoof-plasmon hexamer structure (HS). (c) Enhancement of total radiation efficiency versus frequency for the spoof-plasmon HS. Simulated 3D radiation patterns (d) and measured E plane (e) and H plane (f) of the radiation pattern of the DA coupled with the spoof-plasmon HS.

III. CONCLUSIONS

We demonstrate experimentally spoof-plasmon antennas with fourfold and sixfold rotational symmetries that enable polarization-independent energy concentration and LDOS enhancement under the excitation of arbitrarily polarized incident waves. A half-wave dipole coupled with these structures can radiate below its original fundamental resonance frequency, with a pronounced enhancement of the radiation efficiency. These structures also preserve the far-field radiation pattern and polarization state of the dipole emitter, irrespective of its orientation. This design scheme for polarization-independent radiation management can be extended to other spoof-plasmonic structures with higher-fold ($n \geq 4$) rotational symmetries.

ACKNOWLEDGMENTS

This work is supported, in part, by the National Science Foundation of China under Grants No. 61871127 and No. U21A20459, the 111 Project under Grant No. 111-2-05, and the Fund for International Cooperation and Exchange of the National Natural Science Foundation of China Grant No. 61761136007. Y.L. received funding from the Singapore Ministry of Education [Grant No. MOE2018-T2-2-189(S)], an A*Star AME IRG grant (Grant No. A20E5c0095) and Programmatic Funds (Grant

No. A18A7b0058), and the National Research Foundation Singapore Competitive Research Program (Grants No. NRF220 CRP22-2019-0006 and No. NRF-CRP23-2019-0007).

- [1] M. Agio and D. M. Cano, The Purcell factor of nanoresonators, *Nat. Photonics* **7**, 674 (2013).
- [2] H. Cang, Y. Liu, Y. Wang, X. Yin, and X. Zhang, Giant suppression of photobleaching for single molecule detection via the Purcell effect, *Nano Lett.* **13**, 5949 (2013).
- [3] L. Novotny, Effective Wavelength Scaling for Optical Antennas, *Phys. Rev. Lett.* **98**, 266802 (2007).
- [4] S. V. Boriskina and L. Dal Negro, Multiple-wavelength plasmonic nanoantennas, *Opt. Lett.* **35**, 538 (2010).
- [5] J. B. Pendry, A. Aubry, D. R. Smith, and S. A. Maier, Transformation optics and subwavelength control of light, *Science* **337**, 549 (2012).
- [6] K. Höflich, M. Becker, G. Leuchs, and S. Christiansen, Plasmonic dimer antennas for surface enhanced Raman scattering, *Nanotechnology* **23**, 185303 (2012).
- [7] D. K. Gramotnev and S. I. Bozhevolnyi, Nanofocusing of electromagnetic radiation, *Nat. Photonics* **8**, 13 (2014).
- [8] X. Chen, N. C. Lindquist, D. J. Klemme, P. Nagpal, D. J. Norris, and S.-H. Oh, Split-wedge antennas with sub-5 nm gaps for plasmonic nanofocusing, *Nano Lett.* **16**, 7849 (2016).
- [9] Y. Luo, J. B. Pendry, and A. Aubry, Surface plasmons and singularities, *Nano Lett.* **10**, 4186 (2010).

- [10] K. Li, M. I. Stockman, and D. J. Bergman, Self-Similar Chain of Metal Nanospheres as an Efficient Nanolens, *Phys. Rev. Lett.* **91**, 227402 (2003).
- [11] A. Kogo, Y. Takahashi, N. Sakai, and T. Tatsuma, Gold cluster–nanoparticle diad systems for plasmonic enhancement of photosensitization, *Nanoscale* **5**, 7855 (2013).
- [12] H. Su, X. Shen, G. Su, L. Li, J. Ding, F. Liu, P. Zhan, Y. Liu, and Z. Wang, Efficient generation of microwave plasmonic vortices via a single deep-subwavelength meta-particle, *Laser Photonics Rev.* **12**, 1800010 (2018).
- [13] P. Mühlischlegel, H.-J. Eisler, O. J. F. Martin, B. Hecht, and D. W. Pohl, Resonant optical antennas, *Science* **308**, 1607 (2005).
- [14] T. H. Taminiau, F. D. Stefani, F. B. Segerink, and N. F. van Hulst, Optical antennas direct single-molecule emission, *Nat. Photonics* **2**, 234 (2008).
- [15] J.-J. Greffet, M. Laroche, and F. Marquier, Impedance of a Nanoantenna and a Single Quantum Emitter, *Phys. Rev. Lett.* **105**, 117701 (2010).
- [16] K. A. Willets and R. P. Van Duyne, Localized surface plasmon resonance spectroscopy and sensing, *Annu. Rev. Phys. Chem.* **58**, 267 (2007).
- [17] H. A. Atwater and A. Polman, Plasmonics for improved photovoltaic devices, *Nat. Photonics* **9**, 205 (2010).
- [18] M. Kauranen and A. V. Zayats, Nonlinear plasmonics, *Nat. Photonics* **6**, 737 (2012).
- [19] S. Kühn, U. Häkanson, L. Rogobete, and V. Sandoghdar, Enhancement of Single-Molecule Fluorescence Using a Gold Nanoparticle as an Optical Nanoantenna, *Phys. Rev. Lett.* **97**, 017402 (2006).
- [20] J. B. Pendry, L. Martín-Moreno, and F. J. Garcia-Vidal, Mimicking surface plasmons with structured surfaces, *Science* **305**, 847 (2004).
- [21] A. Pors, E. Moreno, L. Martín-Moreno, J. B. Pendry, and F. J. Garcia-Vidal, Localized Spoof Plasmons Arise while Texturing Closed Surfaces, *Phys. Rev. Lett.* **108**, 223905 (2012).
- [22] Z. Gao, F. Gao, H. Xu, Y. Zhang, and B. Zhang, Localized spoof surface plasmons in textured open metal surfaces, *Opt. Lett.* **41**, 2181 (2016).
- [23] P. Qin, Y. Yang, M. Y. Musa, B. Zheng, Z. Wang, R. Hao, W. Yin, H. Chen, and E. Li, Toroidal localized spoof plasmons on compact metadisks, *Adv. Sci.* **5**, 1700487 (2018).
- [24] Z. Gao, L. Wu, F. Gao, Y. Luo, and B. Zhang, Spoof plasmonics: From metamaterial concept to topological description, *Adv. Mater.* **30**, 1706683 (2018).
- [25] Z. Gao, F. Gao, Y. Zhang, H. Xu, Y. Luo, and B. Zhang, Forward/backward switching of plasmonic wave propagation using sign-reversal coupling, *Adv. Mater.* **29**, 1700018 (2017).
- [26] Z. Liao, J. N. Zhou, G. Q. Luo, M. Wang, S. Sun, T. Zhou, H. F. Ma, T. J. Cui, and Y. Liu, Microwave-Vortex-Beam Generation Based on Spoof-Plasmon Ring Resonators, *Phys. Rev. Appl.* **13**, 054013 (2020).
- [27] G. Su, H. Su, L. Hu, Z. Qin, X. Shen, J. Ding, F. Liu, M. Lu, P. Zhan, and Y. Liu, Demonstration of microwave plasmonic-like vortices with tunable topological charges by a single metaparticle, *Appl. Phys. Lett.* **118**, 241106 (2021).
- [28] Y. Huang, J. Zhang, T. J. Cui, Z. Liao, and D. H. Zhang, Revealing the physical mechanisms behind large field enhancement in hybrid spoof plasmonic systems, *J. Opt. Soc. Am. B* **35**, 396 (2018).
- [29] J. Zhang, Z. Liao, Y. Luo, X. Shen, S. A. Maier, and T. J. Cui, Spoof plasmon hybridization: Spoof plasmon hybridization, *Laser Photonics Rev.* **11**, 1600191 (2017).
- [30] S. M. Hanham, A. I. Fernández-Domínguez, J. H. Teng, S. S. Ang, K. P. Lim, S. F. Yoon, C. Y. Ngo, N. Klein, J. B. Pendry, and S. A. Maier, Broadband terahertz plasmonic response of touching InSb disks, *Adv. Mater.* **24**, OP226 (2012).
- [31] L. Chen, N. Xu, L. Singh, T. Cui, R. Singh, Y. Zhu, and W. Zhang, Defect-induced Fano resonances in corrugated plasmonic metamaterials, *Adv. Opt. Mater.* **5**, 1600960 (2017).
- [32] H. Yu, C. Wang, F.-Y. Meng, J.-G. Liang, H. S. Kashan, K. K. Adhikari, L. Wang, E.-S. Kim, and N.-Y. Kim, Design and analysis of ultrafast and high-sensitivity microwave transduction humidity sensor based on belt-shaped MoO₃ nanomaterial, *Sens. Actuators, B* **304**, 127138 (2020).
- [33] H. Y. Y. Nyein, L.-C. Tai, Q. P. Ngo, M. Chao, G. B. Zhang, W. Gao, M. Bariya, J. Bullock, H. Kim, H. M. Fahad, and A. Javey, A wearable microfluidic sensing patch for dynamic sweat secretion analysis, *ACS Sens.* **3**, 944 (2018).
- [34] A. H. Panaretos and D. H. Werner, Spoof plasmon radiation using sinusoidally modulated corrugated reactance surfaces, *Opt. Express* **24**, 2443 (2016).
- [35] A. Kianinejad, Z. N. Chen, L. Zhang, W. Liu, and C.-W. Qiu, Spoof plasmon-based slow-wave excitation of dielectric resonator antennas, *IEEE Trans. Antennas Propag.* **64**, 2094 (2016).
- [36] A. Kianinejad, Z. N. Chen, and C.-W. Qiu, A single-layered spoof-plasmon-mode leaky wave antenna with consistent gain, *IEEE Trans. Antennas Propag.* **65**, 681 (2017).
- [37] D.-F. Guan, P. You, Q. Zhang, Z.-H. Lu, S.-W. Yong, and K. Xiao, A wide-angle and circularly polarized beam-scanning antenna based on microstrip spoof surface plasmon polariton transmission line, *Antennas Wirel. Propag. Lett.* **16**, 2538 (2017).
- [38] J. Zhang, H.-C. Zhang, X.-X. Gao, L.-P. Zhang, L.-Y. Niu, P.-H. He, and T.-J. Cui, Integrated spoof plasmonic circuits, *Sci. Bull.* **64**, 843 (2019).
- [39] M. Navarro-Cia and S. A. Maier, Broad-band near-infrared plasmonic nanoantennas for higher harmonic generation, *ACS Nano* **6**, 3537 (2012).
- [40] A. Kinkhabwala, Z. Yu, S. Fan, Y. Avlasevich, K. Müllen, and W. E. Moerner, Large single-molecule fluorescence enhancements produced by a bowtie nanoantenna, *Nat. Photonics* **3**, 654 (2009).
- [41] P. Biagioni, J. S. Huang, L. Duò, M. Finazzi, and B. Hecht, Cross Resonant Optical Antenna, *Phys. Rev. Lett.* **102**, 256801 (2009).
- [42] See the Supplemental Material at <http://link.aps.org/supplemental/10.1103/PhysRevApplied.18.054018> for details of the fabricated samples and more simulation results.